**Electronic Supplementary Information**

# Enzyme-responsive Nanoparticles: Enhancing Endolysins' Ability to Eradicate Staphylococcus aureus Biofilm

Mariana Blanco Massani [a], Dennis To [a], Susanne Meile [b], Mathias Schmelcher [b], Débora C. Coraça-Huber [c], Anna Seybold [d], Martin Loessner [b], and Andreas Bernkop-Schnürch [a†]

[a] Centre for Chemistry and Biomedicine (CCB), Department of Pharmaceutical Technology, Institute of Pharmacy, University of Innsbruck, Innrain 80/82, 6020 Innsbruck, Austria

[b] Institute of Food, Nutrition and Health, ETH Zürich, Schmelzbergstrasse 7, 8092 Zürich, Switzerland

[c] Biofilm Lab, Experimental Orthopedics, University Hospital for Orthopaedics and Traumatology, Medical University Innsbruck, Müllerstrasse 44, 1. Floor, 6020 Innsbruck, Austria

[d] Department of Zoology, University of Innsbruck, 6020, Innsbruck, Austria

†Andreas.Bernkop@uibk.ac.at

**Methods/Experimental**

**Materials**

Sodium polyphosphate (PP, Graham's salt, n = 25, Merck, Austria); glycerol 99.0% (Merck, Austria), alkaline phosphatase (Sigma Aldrich, Germany), p-nitrophenyl phosphate (Sigma Aldrich, Germany); $MgCl_2$ (Sigma Aldrich, Germany) 2-amino-2methyl-1propanol (Merck, Austria); TrypLE ™ (Fisher Scientific, Germany); DNase I (Fisher Scientific, Germany), TSB (Carl Roth), violet crystal (Merck, Austria) , $NaIO_4$ (Merck, Austria); resazurin sodium salt (Merck, Austria);phosphate buffer solution (PBS, Fisher Scientific, Germany); inhouse made implant discs DIN9021, stainless steel A2.

**Microorganisms and Growth Conditions**

*Staphylococcus aureus* ATCC 25923 (methicillin sensitive) was provided by the Biofilm Lab (Experimental Orthopaedics, Department of Orthopaedic Surgery, Medical University Innsbruck). Bacterial stock was stored at -20 °C in glycerol and grown in TSB (Carl Roth) at 37 °C under shaking.

**Enzybiotics**

Chimeric PGH M23LST(L)_SH3b2638A (M23) (27.414 KDa, M23) is composed of an M23 endopeptidase domain from lysostaphin and an SH3b cell wall binding domain (CBD) from phage 2638A endolysin [1]. CHAPGH15_SH3bALE1 (29.964 KDa, GH15), consists of a CHAP endopeptidase domain from LysGH15 and an SH3b CBD from ALE1 [1,2].

Chimeric endolysins were expressed in *E. coli*, purified as previously described [3–5], and lyophilized. The fractions stored at -20 °C were resolubilized in water before the experiments.

Calculation of protein parameters and in silico modelling was performed using Protparam tool and SWISS-MODEL from Expasy [6], while calculation of charge at different pH was performed using Protpi program (https://www.protpi.ch/Calculator/ProteinTool#Results).

**Polyphosphate Nanoparticles Formation and Characterization**

Chimeric endolysins-PP NPs were obtained by ionotropic gelation, which is based on the electrostatic interactions of oppositely charged phage endolysins and PP. [7] For this, PP, M23 and GH15 solutions were prepared in different concentrations and pHs as detailed in Table S1 and incubated for 15 minutes at 1000 rpm at 24 °C using a thermomixer (Eppendorf, Germany). Thereafter, 350 µl of solution of each chimeric endolysin was added dropwise to 350 µl solutions of PP and left under constant shaking for 10 minutes at these conditions.

Mean dynamic particle size (DS), size distribution and zeta potential of the obtained nanoparticles were obtained by dynamic and electrophoretic light scattering techniques using Zetasizer Nano (ZSP, Malvern Instruments, Worcestershire, UK). All measurements were performed at 24 °C in independent triplicates. Data fitting algorithms and analysis [8] was provided by

Zetasizer Software 8.02 Copyright© 2002-2021 Malvern Panalytical. All the data used in this work meets the Malvern Instruments quality criteria for a measurement.

Energy-filtered transmission electron microscopy (EFTEM) was used to visually confirm the presence PGH-PP NPs. For this, 5ul of each freshly prepared sample were mounted on a Formvar/carbon-coated copper grid (Balzers Union, Liechtenstein) of 200 mesh. After drying, samples were analysed with a Zeiss Libra 120 (Carl Zeiss AG, Oberkochen, Germany). Images were taken using a 2 x 2 k highspeed camera (Troendle, Germany) and ImageSP software (Troendle, Germany).

**Minimum Inhibitory Concentration (MIC) and Minimum Bactericidal Concentration (MBC)**

Chimeric endolysins M23 and GH15, and their PP NPs were assayed for MIC against planktonic *S. aureus* strains by the broth dilution method. [9] For this, 2-fold dilutions of the antimicrobials were seeded together with $10^5$ CFU/mL *S. aureus* in a 96 well plate. Absorbance at 620 nm was measured after incubation (18-21 h at 37 °C). MIC was defined as the lowest endolysin concentration (nM) resulting in no turbidity. Thereafter, 100 µl of sample from wells showing no turbidity were plated on TSA and incubated (48 h at 37 °C). The concentration of endolysins (nM) reducing the bacteria by 99.9% was defined as the MBC. [10]

**Technological Properties of NP Formulations**

Freshly prepared endolysin-PP NPs were stored at 4 °C. At different time points, DS, zeta potential and MIC were determined. Cytotoxicity was evaluated via the resazurin assay as detailed elsewhere. [11] Caco-2 (immortalized cell line of human colorectal adenocarcinoma) and HeLa (immortalized cell line of human cervical carcinoma) were seeded ($2 \times 10^4$ cells/well) in a 96 well plates and grown to 90-100% confluency at 37 °C under 5 % CO2 and 95 % relative humidity. PBS was used for application of free PGHs and PGH-PP in five replicates, reaching final concentrations of PGHs of 312.5, 156.3, 78.3, 39.1 nM. Buffer only served as positive control, while a 0.1% Triton X-100 solution served as negative control. After 2 h of incubation, samples were removed and 100 µl of an 8.8 µM resazurin solution was applied to each well. After 2 h of incubation at the above-mentioned conditions, fluorescence ($\lambda_{Ex}$ 540 nm, $\lambda_{Em}$ 590 nm) was determined using Tecan Spark microplate reader. Cell viability was calculated using Equation (1).

$$Cell\ viability\ (\%) = \frac{Intensity(Sample) - Intensity(Negative\ control)}{Intensity(Positive\ control) - Intensity(Negative\ control)} \times 100\%$$

Stability to serine protease activity was determined using TrypLE™ recombinant enzyme as a surrogate. M23 enzyme was used for this experiment, given its low MIC compared to GH15 and its initial nanoscale size. 625 nM M23-PP NPs and free M23 were treated for 20 minutes at 37 °C with TrypLE and heat inactivated TrypLE in a ratio of 1:2 (final concentration 312.5 nM). Thereafter, MIC was determined for all the samples.

**Establishment of Biofilm in Implants**

Three colonies of *S. aureus* ATCC 25923 were inoculated in TSB and grown overnight during 18-24 h at 37 °C, under shaking. The culture was transferred to TSB and incubated for 1 h to reach exponential growth at 37 °C, under shaking. After this, 16 pieces of stainless-steel implant samples (141.3 $mm^2$) were placed in a 6 well plate and inoculated with 3 ml TSB supplemented with glucose (1%) containing *ca.* $10^5$ CFU/ml. This setup was incubated at 37 °C, under shaking at 100 rpm for 18-21 h. Unless indicated otherwise, the implants with grown biofilm were deeply rinsed with physiological solution to remove planktonic bacteria. Implant samples grouped in 4 pieces were assessed for biomass, AP activity, and counting according to the description given below.

**Alkaline Phosphatase (AP) Activity**

AP activity in biofilm was determined colorimetrically by the hydrolysis of p-nitrophenyl phosphate in buffer containing $MgCl_2$ (5 µM) and 2-amino-2-methyl-1-propanol (0.5 M) (pH 9) (D. To *et al.* unpublished experiments). A calibration curve using AP was performed. All samples were incubated with the substrate for 1 h at 37 °C. Absorbance was measured in triplicate at 450 nm.

**Cell Counting**

Implant samples were incubated with TrypLE at 37 °C for 15 minutes under shaking. [12] TSB was added, thoroughly vortexed, and dilutions ($10^{-1}$$10^{-8}$) were plated on TSA. Cells were counted after 48 h incubation at 37 °C and expressed as colony forming units (CFU) per $cm^2$ of implant surface.

**SEM Analyses**

*S. aureus* ATCC 25923 biofilms grown on sterile stainless-steel disc were morphologically characterized using SEM before and after treatments with water (control), PGHs and PGH-PP NPs. First, samples were fixed for 24 h at 4 °C in 2 ml of glutaraldehyde 2.5%. Dehydration process after fixation was performed with an ascending alcohol series (50%–70%–80%–99.9% ethanol). Each step lasted 5 min. The dried samples were mounted on aluminium pins using carbon adhesives. The pins were sputtered with Au using an automatic sputter coater (Agar Scientific Ltd, Stansted, UK) for 45 seconds and analysed by scanning electron microscopy (SEM, JSM-6010LV, JEOL GmbH, Freising, Germany). [13]

**Time-Kill Assay**

The biofilm formed on implant surface was treated with water or HCl 0.02 M (control), free chimeric endolysins or the respective PGH-PP NPs. At time 0, and after 1 h, 2 h and 4 h of treatment all samples were assessed by cell counting in 2 replicates. The times producing the highest decreases in bacterial counts were repeated in a second independent replicate and assessed for SEM imaging, and AP activity.

**Enzyme-Triggered Release**

*S. aureus* ATCC 25923 biofilm grown on an implant surface was treated for 1 h with sterile inorganic phosphate buffer ($P_i$) at isotonic concentration ($NaH_2PO_4$ 0.11642 M and $Na_2HPO_4$ 0.12758 M, pH 7). Afterwards, the medium was replaced with 312.5 nM M23-PP NPs or M23 mixed with $P_i$ in a 1:1 ratio. Samples were incubated for 2 h at 37 °C under shaking (100 rpm). Thereafter, AP activity and CFU were determined as detailed above.

**Statistical Analysis**

Data was analysed using GraphPad Prism 5 (GraphPad Software, Inc., San Diego, CA, USA). One-way ANOVA and two-way Bonferroni multiple comparison tests were applied, and statistical significance was defined as $p<0.05$ probability values.

**Additional electronic supplementary information**

Raw data supporting the findings of this publication are included as xls files as detailed: Raw data for size, and PDI under different screening conditions for developing PGH-PP NPs corresponding to **Figure 1** and Table S1 (PGH-PP-NPs_Screening conditions.xls); zeta potential of the most promising formulations of PGH-PP NPs, corresponding to **Figure 1** (PGH-PP-NPs Zeta potential.xls); MIC and MBC of free PGH and PGH-PP NPs corresponding to **Figure 2A** (MIC and MBC.xls); percentage of viability after exposure of Caco2 to formulations of free PGH and PGH-PP NPs corresponding to **Figure S2** (Cytotoxicity towards Caco2 and HeLa.xls); size and zeta potential form PGH-PP NPs stored at 4°C corresponding to **Figure 2B** and **C** (Stability over storage time.xls); MIC after treatment of M23 and M23-PP NPs with serine protease for 20 minutes at 37°C corresponding to **Figure 3** (PGH-PP-NPs Protective effect.xlsx); colony forming units over time after treatment of S. aureus 25923 biofilm with 156.3 nM M23 and M23-PP NPs corresponding to **Figure 4A** (M23 and M23-PP-NPs Time-kill.xlsx); AP activity over time after treatment of *S. aureus* 25923 biofilm with 156.3 nM M23 and M23-PP NPs corresponding to **Figure 4D** (AP Activity-M23 Time-kill.xls); colony forming units over tie after treatment of S. aureus 25923 biofilm with 625 nM GH15 and GH15-PP NPs corresponding to **Figure 5A**. Manuscript (GH15 and GH15-PP-NPs Time-kill.xlsx); AP activity over time after treatment of *S. aureus* 25923 biofilm with 625 nM GH15 and GH15-PP NPs corresponding to **Figure 5D** (AP Activity-GH15 Time-kill.xls); colony forming units after treatment of S. aureus biofilm with M23, PP-M23 NPs and control in the presence and absence of inorganic phosphate (Pi). corresponding to **Figure 6** (Enzyme-Triggered Antistaphylococcal Activity.xls)

**Screening conditions for peptidoglycan hydrolase polyphosphate (PGH-PP) NPs formation.** Chimeric PGHs were solubilized at different pH conditions (Table S1). In order to define the protein to PP ratio, the charge of enzybiotics was predicted *in silico*. Ratios from 1:1 to 1:7 were screened, depending on the enzybiotic and considering that PP (n = 25) negative charges are derived from monovalent negative charge of each internal P-subunit ($pK_a$ = ~0–3) [7]. Protein concentration for NPs formation was screened using CHAPGH15_SH3bALE1 chimeric endolysin (GH15, 29.964 KDa, *Iep* 8.801) from 5 µM to 1.25 µM. The presence of buffer in the formulations increased the ionic strength of the system, which led formation of agglomerates (Table S1). Therefore, water-based formulations were chosen for further NPs development.

M23-LST(L)_SH3b2638 chimeric PGH (M23, 27.414 KDa, *Iep* 8.44), presented different solubilities at different pHs (Table S1). The endolysin solution was turbid with a particle size of 373 ± 134 nm, PDI 0.50 ± 0.13 at pH 7.4, while at pH 5 an opalescent suspension was observed (particle size of 948.5 ± 134, PDI 0.57 ± 0.08) that turned to be transparent at pH 2 (particle size of 146.2 ± 16.29 nm, PDI 0.33 ± 0.06). NPs were formulated at acidic pH, as more stable positively charged NPs of chimeric M23 were formed under this condition.

The most promising formulations showing mean dynamic particle size (DS) lower than 300 nm and a PDI lower than 0.3 are presented in **Figure 1** and **2** (main manuscript).

**Table S1**. Screening conditions for PGH-PP NPs formation

| Formulation code | Cation concentration | Cation net charge at (pH) | PP concentration | Ratio cation to PP (µMol) | Media used for formulation | Ultrasonication | Formulation ionic strength | Outcome | Size (nm) | PDI |
|---|---|---|---|---|---|---|---|---|---|---|
| F0 | GH15 5µM | +3.644 (7.4) | 0 | NA | Water | No | 0.046925 | Transparent solution | NA | NA |
| F1pbs | GH15 5µM | | 15 µM | 1:3 | PBS pH 7.4 | Yes | 0.59121 | Macroscopic phase separation | NA | NA |
| F2pbs | | | 20 µM | 1:4 | | Yes | 0.65121 | Macroscopic phase separation | NA | NA |
| F3pbs | | | 25 µM | 1:5 | | Yes | 0.71121 | Macroscopic phase separation | NA | NA |

| | | | | | | | | | | |
|---|---|---|---|---|---|---|---|---|---|---|
| F1w | | | 15 µM | 1:3 | water | Yes | 0.267786 | Opalescent suspension | 2496 ± 39 | 0.345 ± 0.051 |
| F2w | | | 20 µM | 1:4 | | Yes | 0.297786 | Opalescent suspension | 2927 ± 9 | 0.349 ± 0.028 |
| F3w | | | 25 µM | 1:5 | | Yes | 0.327786 | Opalescent suspension | 3304 ± 100 | 0.436 ± 0.093 |
| F1w-1 | GH15 2.5 µM | | 7.5 µM | 1:3 | | | | Opalescent suspension | 912 ± 34 | 0.370 ± 0.008 |
| F2w-1 | | | 10 µM | 1:4 | | | | Opalescent suspension | 2154 ± 134 | 0.332 ± 0.025 |
| F3w-1 | | | 12.5 µM | 1:5 | | | | Opalescent suspension | 1357 ± 106 | 0.332 ± 0.040 |
| F4w | M23 1.25µM | +1.654 (7.4) | 0 | NA | Water | No | | Turbid suspension | NA | NA |

| | | | | | | | | |
|---|---|---|---|---|---|---|---|---|
| F5hcl | +12.252 (5) | 0 | NA | HCL | No | Turbid suspension | NA | NA |
| F6hcl | +25.92 (1.92) | 0 | NA | HCL | No | Transparent solution | 189 ± 58 | 0.434 ± 0.049 |
| F6hcl-1 | | 1.25 µM | 1:1 | HCL | No | Opalescent suspension | 90 ± 16 | 0.606 ± 0.147 |
| F6hcl-3 | | 3.75 µM | 1:3 | HCL | No | Opalescent suspension | 57 ± 4 | 0.533 ± 0.080 |

NA, not applicable

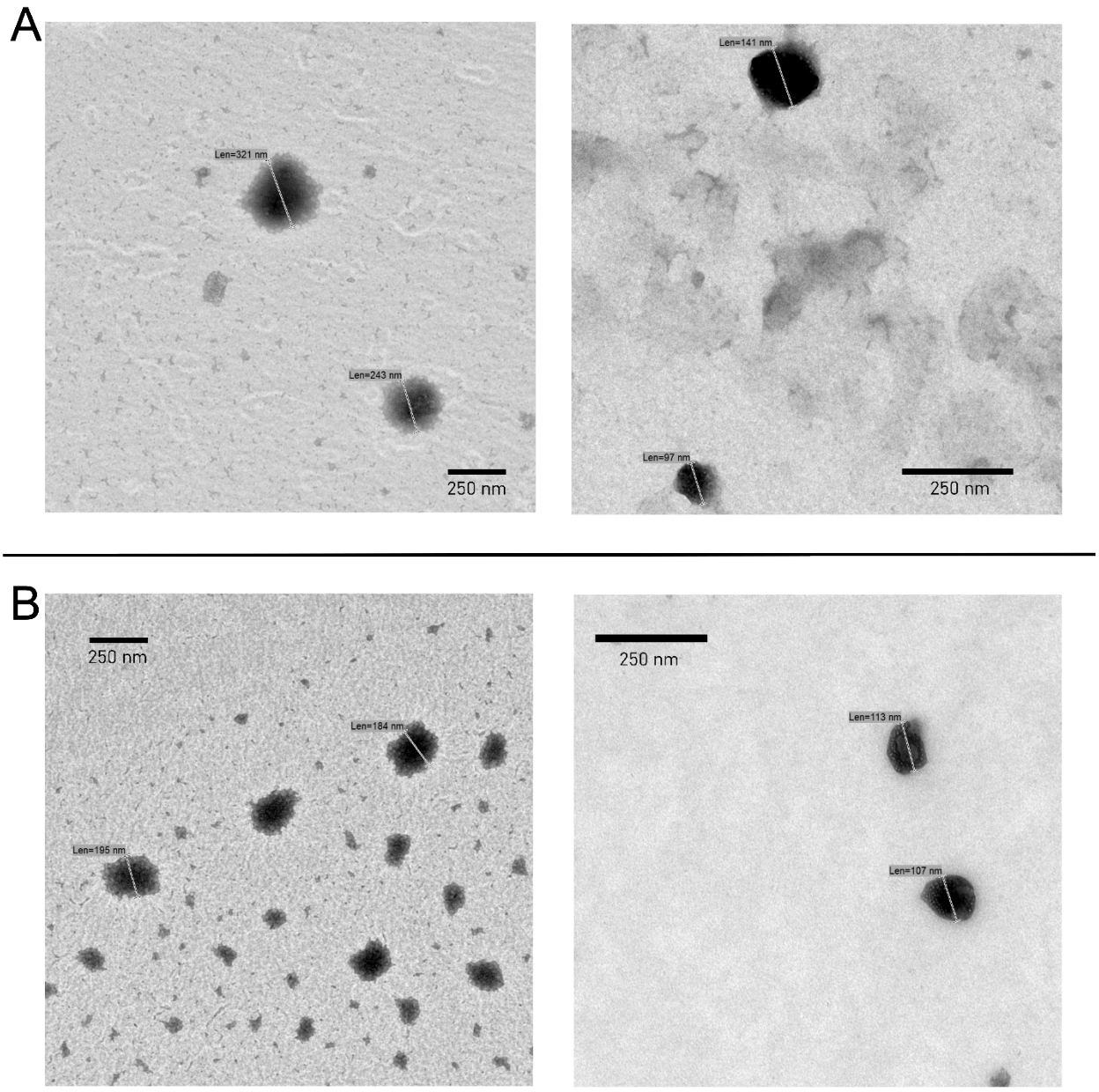


**Figure S1.** (A) M23-PP NPs, M23 to PP ratio 1:7 and (B) GH15-PP NPs, GH15 to PP ratio 1:5 analyzed by TEM were in coincidence with the DS and PDI described in **Figure 1** (main manuscript). The presence of GH15-PP NPs of smaller dimensions than those found by DLS (Figure 1B, main manuscript) can be explained by the differences in the fundaments of both complementary characterization techniques.[8,14]

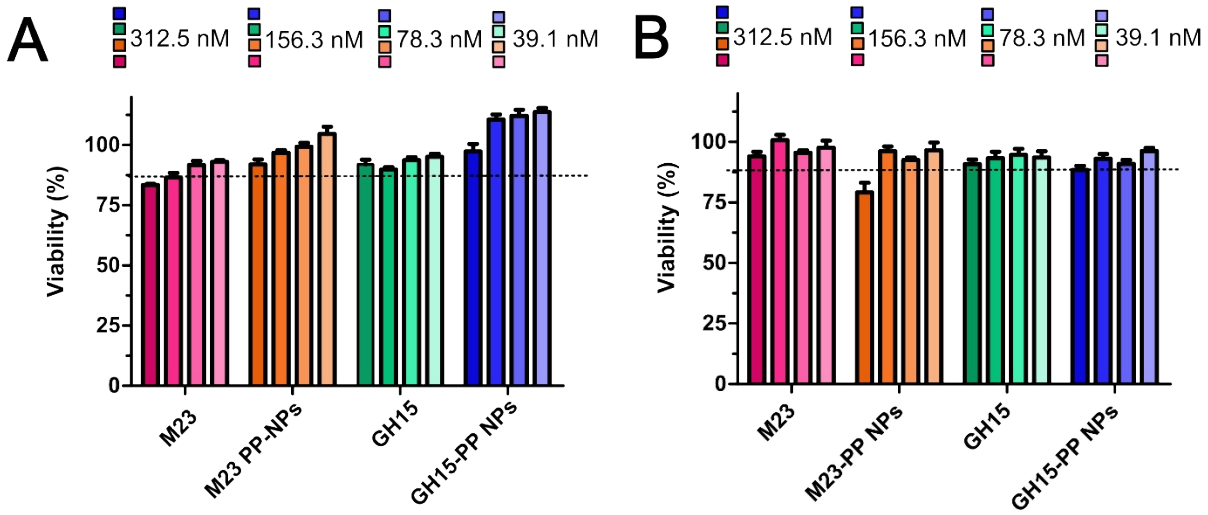


**Figure S2.** Cell viability for free and encapsulated PGHs towards (A) Caco2 and (B) HeLa. Indicated values are means (n=5) ± SD. Dotted line in (B) indicates viability around 80%.

**A**

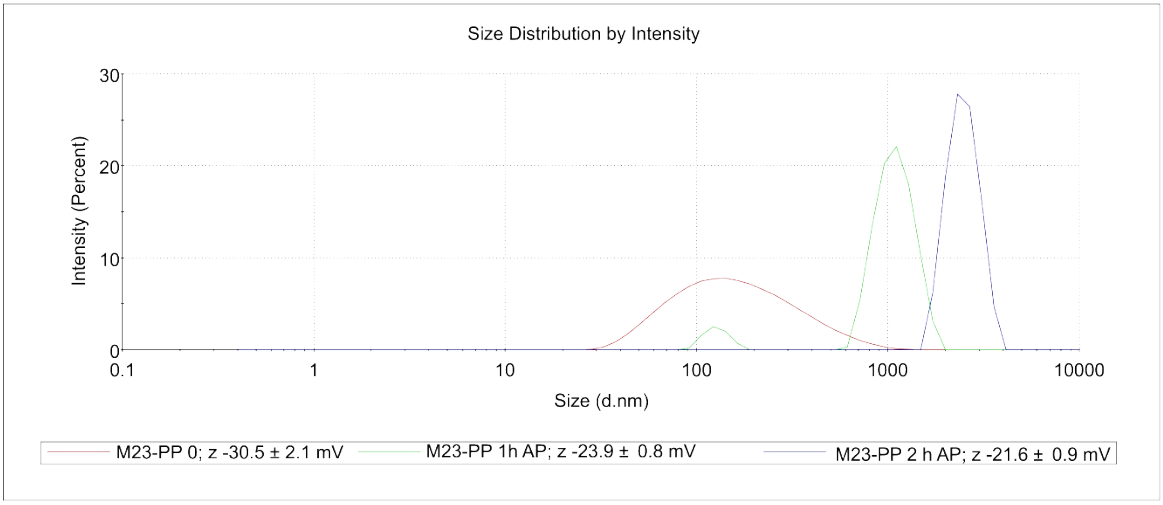


**B**

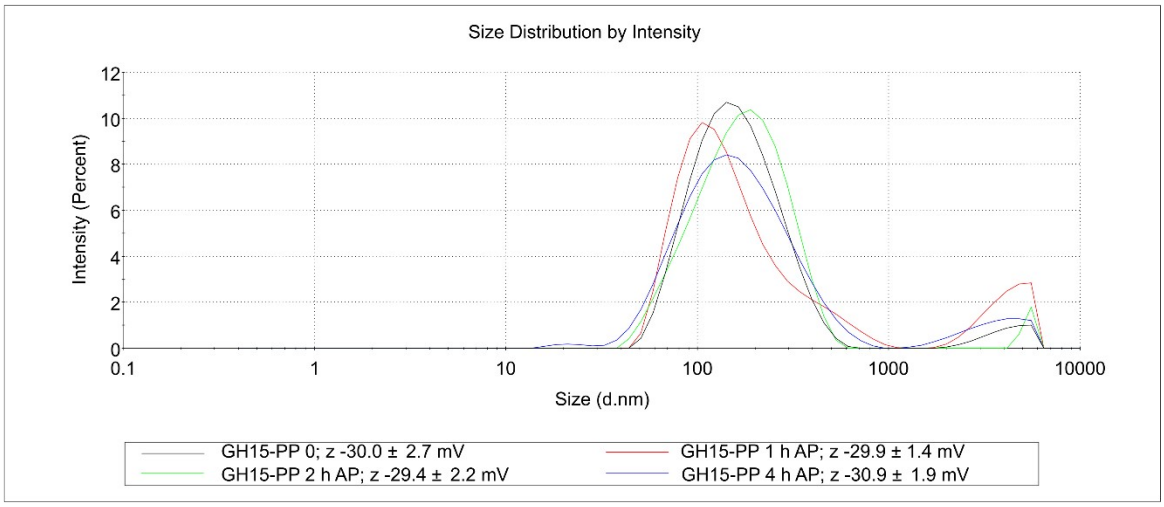


**Figure S3.** PP-GHs NPs size changes upon AP activity for (A) M23-PP, M23 to PP ratio 1:7 and (B) GH15-PP NPs, GH15 to PP ratio 1:5. The corresponding zeta potentials are shown at the foot of each figure.

A pronounced increase in size for PP-M23 and shift in charge to less positive zeta potentials (Δ8.9 mV) was observed upon 2h of AP treatment, confirming the net charge change triggered by AP. The rise in NPs size can be explained by particle aggregation resulting from less repulsion, probably due to increased enrichment in of M23 on the surface of NPs. These results are consistent with the slow phosphate release observed for these NPs (**Figure S3**), which suggests that not all phosphate moieties are located on the surface of these systems being consequently of limited access for phosphatase. [15] Such intercalated structure composed of PP and M23 led to a distribution of particle sizes in the range of 229 ±119 nm (**Figure S1A**) and seems to be beneficial for antimicrobial efficacy, compared to GH15-PP NPs (**Figure 4** compared to **Figure 5** in the main manuscript).

In contrast, upon GH15-PP NPs treatment with AP for 4 hours, less pronounced change in size with non-significant shifts in zeta potential was observed (**Figure S3B**). This, together with a fast phosphate release upon AP treatment (**Figure S3B**), may suggest that polyphosphate moieties are located mostly on the surface of GH15-PP NPs impeding GH15 release; therefore, not reaching the full antimicrobial potential of the NPs after 4 h of incubation with bacterial biofilm (**Figure 5**, main manuscript).

**Phosphate release**. PGH-PP NPs phosphate release triggered by AP was studied for 24h either for the free polymer and the PGH-PP NPs. For this, 1 ml of PP or PP PGHs NPs were formulated at the same conditions regarding pH and polymer concentration (i.e. pH 1.92 and PP 4.375 µM for Figure S3A, and pH 7.4 PP 3.125 µM) and placed in a dialysis tube (cut off 100-500 Da) and incubated at 37°C, under 150 rpm shaking, with HEPES buffer (control) or 0. 0006 DEA/ ml AP in HEPES. Samples were removed at 1h, 2h, 4 h and 24h, and phosphate release was determined by malachite green as previously reported.[7]

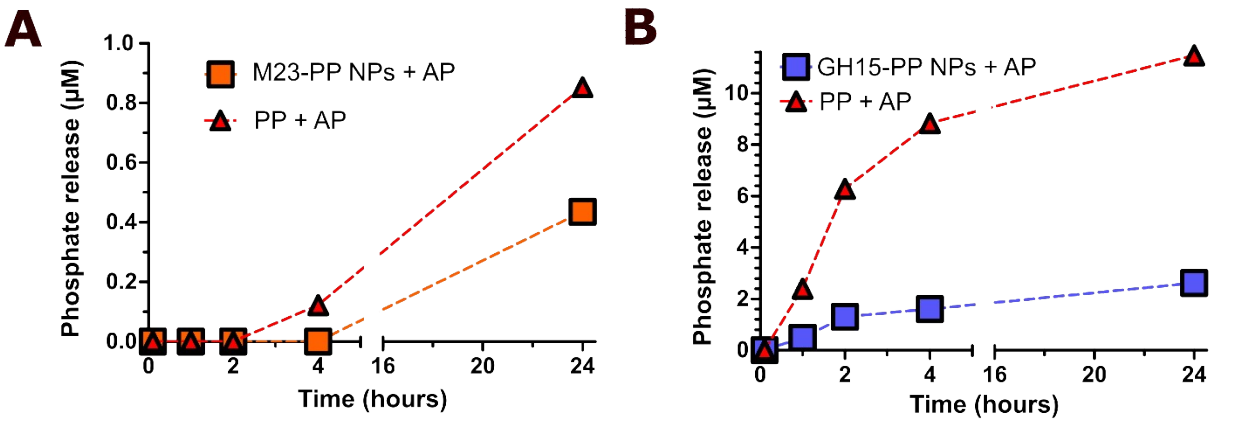


**Figure S4.** Phosphate release upon treatment with AP at 37°C for (A) M23-PP NPs, protein to polymer 1:7 and polymer only at pH 3 and (B) GH15-PP, protein to polymer 1:5. Free PP in each figure (red triangles) to the concentration of PP and the pH of the corresponding formulation.

As depicted in **Figure S4B**, phosphate release triggered by AP was detected for GHPP 15-NPs from 1 h of incubation, and it increased over time. The same behavior was observed for phosphate release from PP treated with AP. For all the measurements, hepes buffer treatment showed no detectable phosphate release. This behavior was accompanied by with particles agglomeration after treatment (**Figure S3B**), confirming the proper positioning of polyphosphate groups AP cleavage, since either for the free polymer or for the NPs phosphate is release after 1 h incubation time.[15] The difference between the phosphate concentration released by PP and PPGH15 can be attributed to a more packed structure in NPs compared to the free polymer, as previously found for PP NPs. [16]

Notably, the fast release of phosphate is in line with steady increase in antimicrobial efficacy from 1 to 4 h when biofilm is treated with GH15-PP NPs (**Figure 5**, main manuscript).

For M23-PP NP, phosphate release was below the detection limit for 1, 2 and 4 h of incubation. However, after 24 h of incubation with AP, 434 nM phosphate was released. Moreover, a delay in release for M23-PP NPs compared to the PP under the same conditions was observed. Less accessibility of phosphate to AP maybe because of an intercalated structure of the NPs may account for this result. Notably, the shift in particle charge and size (**Figure**

**S3A**), together with the increased antimicrobial efficacy reached by M23-PP NPs (**Figure 4**, main manuscript) showed that the NPs with this arrangement were the most effective for AP triggered staphylococcal biofilm eradication. The slower release observed in general in **Figure S3A**, compared to **Figure S3B** is consistent with the low pH of M23-PP and the corresponding PP control (pH 3) which is far from the optimum pH for AP activity.

| Sample | Reduction (%) compared to control | Outcome[17] |
|---|---|---|
| M23-PP pH 1.92 ,625 nM in M23, protein to polymer ratio 1:7 | 100 | Bactericidal |
| PP 4.375 µM pH 1.92 | 93.3 | Bacteriostatic |
| GH15-PP pH 7.4, 625 nM in M23, protein to polymer ratio 1:5 | 100 | Bactericidal |
| PP 3.125 pH 7.4 µM | 89.4 | Bacteriostatic |

**Table S2.** Antimicrobial effect found for PGH-PP NPs, and the free PP as used in each corresponding formulation.

$10^5$ CFU/ml were incubated with PGH-PP NPs, and the free PP overnight as described in the materials and methods section. All the samples showed inhibitory effect with no turbidity detected by OD at 620 nm. However, after counting the cells treated by each sample, inhibition was consistent with a bacteriostatic effect[17] obtained for free PP, in contrast to the bactericidal effect of NPs.

**Evaluation of staphylococcal biofilm composition.** Implant surfaces with grown biofilm were washed with water 3 times. The main extracellular polymeric substances of staphylococcal biofilm (exopolysaccharides, proteins and eDNA) was evaluated by treating the implant surfaces for 15 minutes at 37 °C, under shaking respectively with (i) sodium meta-periodate ($NaIO_4$, 0.04 mol/L in distilled water) for exopolysaccharide; (ii) TrypLE$^{TM}$ recombinant enzyme for protein and (iii) DNase I (100 U/ml) for eDNA determination. The treated samples were stained with 1 ml 0.1% (m/V) crystal violet, deeply washed with demineralized water and air dried. The bound dye was dissolved with 1 ml of 33% glacial acetic acid. Biomass before and after treatments was determined by spectrophotometry at 593 nm. [18]

Changes of biofilm upon different treatments (**Figure S5**) showed the strongest reduction of biomass after TryPLE. Consistent with previous findings, this suggests a biofilm extracellular matrix principally constituted of proteins. [19.] Consequently, the use of TryPLE served for cell counting determination [12] in the present work.

Alkaline phosphatase activity (AP) basal levels in *S. aureus* ATCC 25923 biofilm was 0.006 ± 0.001 DEA/ml.

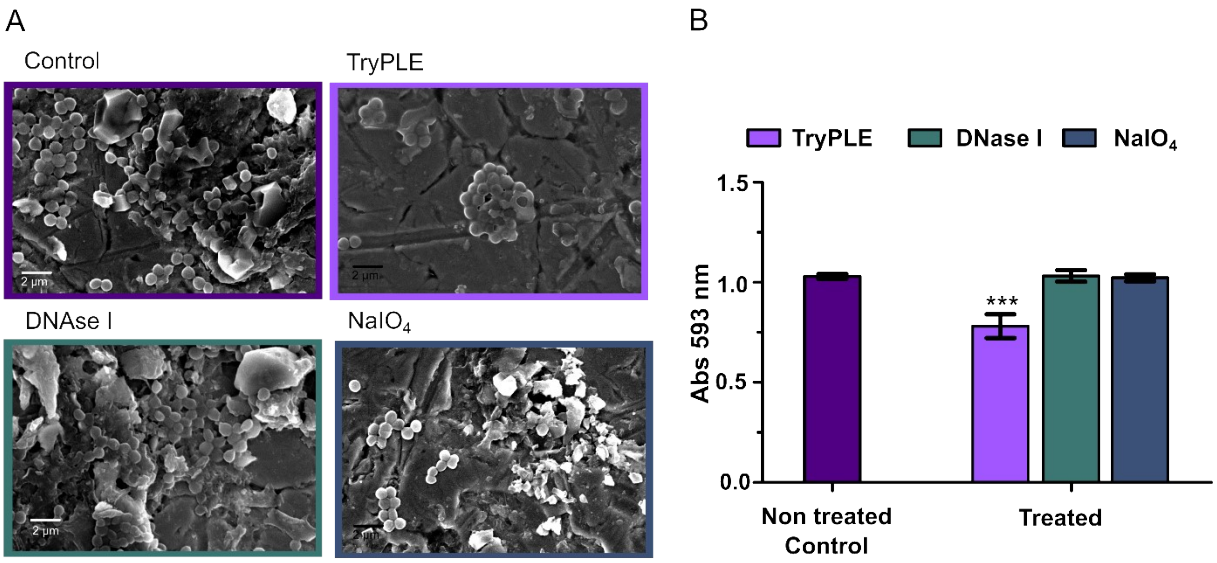


**Figure S5.** (A) Changes in extracellular matrix composition and (B) biomass of *S. aureus* ATCC 25923 biofilm after different treatments.

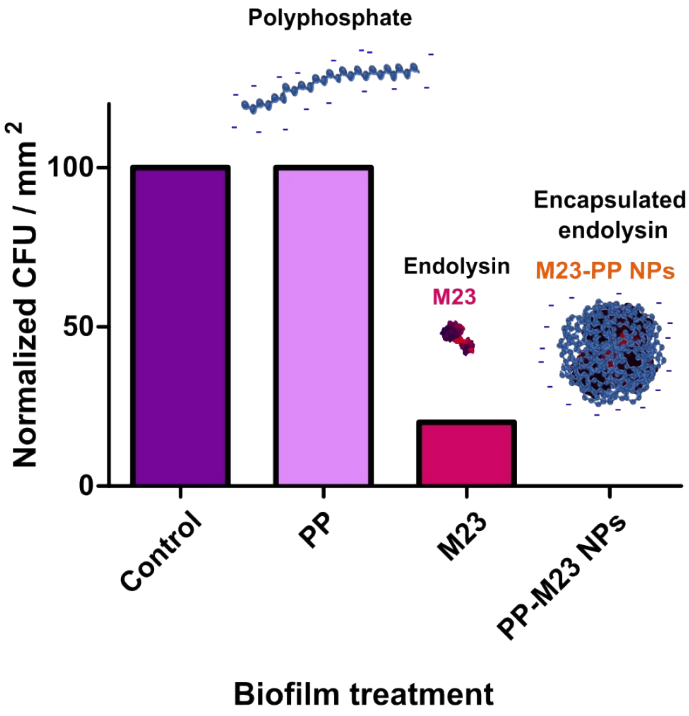


**Figure S6.** Normalized CFU/mm$^2$ of *S. aureus* after biofilm treatment during 1 hour with polyphosphate at the concentration used for preparing NPs (4.375 µM), M23 (625nM) and M23-PP NPs (625nM in M23). While a strong inhibition of bacterial counts was observed for the PGH and the formed NPs, no inhibition was obtained upon treatment with polyphosphate.

**AP variation upon inorganic phosphate (Pi) onset.** Biofilm treated with $P_i$ for 1 h and subsequently with the different treatments supplemented with $P_i$ (**Figure S7**) showed similar reduction of AP activity.

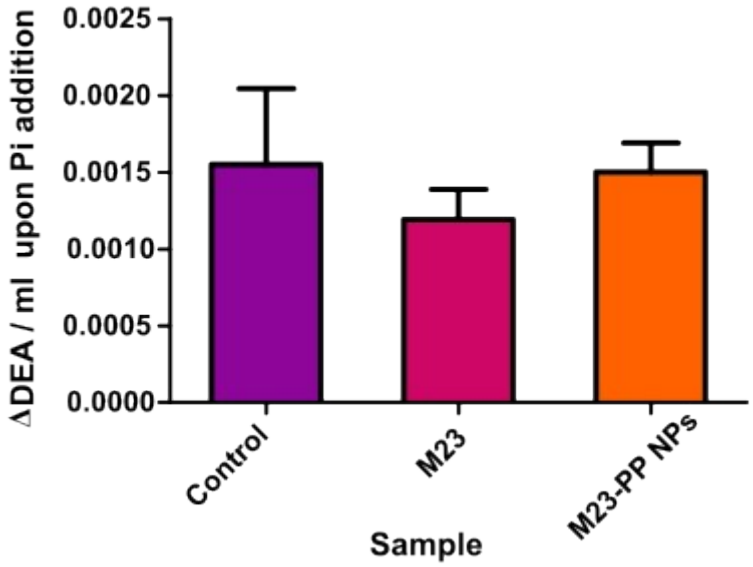


**Figure S7**. Alkaline phosphatase activity variation upon onset of $P_i$ in biofilm treated with different samples.

**References**


1 M. Schulz, S. Calabrese, F. Hausladen, H. Wurm, D. Drossart, K. Stock, A. M. Sobieraj, F. Eichenseher, M. J. Loessner, M. Schmelcher, A. Gerhardts, U. Goetz, M. Handel, A. Serr, G. Haecker, J. Li, M. Specht, P. Koch, M. Meyer, P. Tepper, R. Rother, M. Jehle, S. Wadle, R. Zengerle, F. Von Stetten, N. Paust and N. Borst, *Lab Chip*, 2020, **20**, 2549–2561.

2 C. Röhrig, M. Huemer, D. Lorgé, S. Luterbacher, P. Phothaworn, C. Schefer, A. M. Sobieraj, L. V Zinsli, S. Mairpady Shambat, N. Leimer, A. P. Keller, F. Eichenseher, Y. Shen, S. Korbsrisate, A. S. Zinkernagel, M. J. Loessner and M. Schmelcher, *mBio*, 2020, **11**, 1–19.

3 A. M. Sobieraj, M. Huemer, L. V. Zinsli, S. Meile, A. P. Keller, C. Röhrig, F. Eichenseher, Y. Shen, A. S. Zinkernagel, M. J. Loessner and M. Schmelcher, *mBio*, 2020, **11**, 1–16.

4 M. Schulz, S. Calabrese, F. Hausladen, H. Wurm, D. Drossart, K. Stock, A. M. Sobieraj, F. Eichenseher, M. J. Loessner, M. Schmelcher, A. Gerhardts, U. Goetz, M. Handel, A. Serr, G. Haecker, J. Li, M. Specht, P. Koch, M. Meyer, P. Tepper, R. Rother, M. Jehle, S. Wadle, R. Zengerle, F. Von Stetten, N. Paust and N. Borst, *Lab Chip*, 2020, **20**, 2549–2561.

5 J. Seijsing, A. M. Sobieraj, N. Keller, Y. Shen, A. S. Zinkernagel, M. J. Loessner and M. Schmelcher, *Front Microbiol*, 2018, **9**, 1–9.

6 E. Gasteiger, C. Hoogland, A. Gattiker, S. Duvaud, M. R. Wilkins, R. D. Appel and A. Bairoch, *The Proteomics Protocols Handbook*, 2005, 571–608.

7 Z. B. Akkuş-Dağdeviren, A. Saleh, C. Schöpf, M. Truszkowska, D. Bratschun-Khan, A. Fürst, A. Seybold, M. Offterdinger, F. Marx and A. Bernkop-Schnürch, *J Colloid Interface Sci*, 2023, **646**, 290–300.

8 S. Bhattacharjee, *Journal of Controlled Release*, 2016, **235**, 337–351.

9 E. Committee, S. Testing, C. Microbiology and I. D. Escmid, *Clinical Microbiology and Infection*, 2003, **9**, ix–xv.

10 I. Diseases, *Clinical Microbiology and Infection*, 2000, **6**, 503–508.

11 A. Saleh, Z. B. Akkuş-Dağdeviren, S. Haddadzadegan, R. Wibel and A. Bernkop-Schnürch, *Biomacromolecules*, 2023, **24**, 2587–2595.

12 C. Spiegel, M. Nogler and D. C. Coraça-huber, 2022, 1–10.

13 L. Knabl, B. Kuppelwieser, A. Mayr, W. Posch, M. Lackner, D. Coraça-Huber, A. Danita, M. Blauth, C. Lass-Flörl and D. Orth-Höller, *Microbiologyopen*, 2019, **8**, e00658.

14 S. Mourdikoudis, R. M. Pallares and N. T. K. Thanh, *Nanoscale*, 2018, **10**, 12871–12934.

15 B. Le-Vinh, Z. B. Akkuş-Dağdeviren, N. N. Le, I. Nazir and A. Bernkop-Schnürch, *Adv Ther (Weinh)*, 2022, **5**, 2100219.

16 S. Bonengel, F. Prüfert, G. Perera, J. Schauer and A. Bernkop-Schnürch, *Int J Pharm*, 2015, **483**, 19–25.

17 M. C. Verdi, C. Melian, P. Castellano, G. Vignolo and M. Blanco Massani, *Int J Food Sci Technol*, 2020, **55**, 267–275.

18 J. Azeredo, N. F. Azevedo, R. Briandet, N. Cerca, T. Coenye, A. R. Costa, M. Desvaux, G. Di Bonaventura, M. Hébraud, Z. Jaglic, M. Kačániová, S. Knøchel, A. Lourenço, F. Mergulhão, R. L. Meyer, G. Nychas, M. Simões, O. Tresse and C. Sternberg, *Critical Reviews in Microbiology*, 2017, **43**, 313–351.

19 L. Foulston, A. K. W. Elsholz, A. S. Defrancesco and R. Losick, 2014, **5**, 1–9.